Transverse measurements of polarization in optically pumped Rb vapor cells

J. M. Dreiling,[1] E. B. Norrgard,[1,*] D. Tupa,[2] and T. J. Gay[1]
[1]*Department of Physics and Astronomy, University of Nebraska, Lincoln, Nebraska 68588-0299, USA*
[2]*Los Alamos National Laboratory, Los Alamos, New Mexico 87545, USA*
(Received 13 September 2012; published 26 November 2012)

We have developed a simple heuristic method for determining the polarization of an optically pumped alkali-metal vapor. A linearly polarized probe beam traverses a vapor cell perpendicular to the pump-beam propagation direction, and the transmitted beam intensity is monitored for orthogonal linear polarizations. As the probe beam is scanned in frequency across the D_1 transition, its linear-polarization-dependent transmission can be used as a measure of the atomic orientation of the vapor. We analyze these transmission differences and their dependence on the alkali-metal number density in the vapor.

DOI: 10.1103/PhysRevA.86.053416 PACS number(s): 32.80.Xx

I. INTRODUCTION

Optical pumping of alkali-metal vapor is ubiquitous in atomic physics and is used for a variety of applications. Among these are storage of light [1]; atomic clocks [2] and magnetometers [3]; the production of polarized ions [4–6], neutrons [7], and solids [8]; gas targets for nuclear physics studies [9], and the generation of polarized noble gases through spin-exchange optical pumping [10]. Each of these experiments requires significantly different operating conditions. For example, storage of light in a warm alkali-metal vapor is effected with little or no buffer gas and with spectrally narrow, low-power lasers, while systems that use spin-exchange optical pumping to generate polarized noble gases tend to use high buffer-gas pressures (∼1000 Torr) and broad, high-power lasers. The work reported here deals with a third regime, using somewhat broad, high-power lasers with low pressures (0.1–20 Torr) of buffer gas and an alkali-metal density of 10^{12} to 10^{13} cm^{-3} [11–13]. Among other possible applications, such as gas-cell atomic clocks [14], these conditions are necessary to generate a beam of electrons polarized through spin exchange with a spin-polarized optically pumped alkali-metal target [12]. The necessity of passing the electrons through the alkali-metal (Rb) vapor requires that the buffer-gas pressures be modest to maintain an appreciable electron current. We hope to use this technology to produce a "turnkey" polarized electron source.

The Rb polarization P_{Rb} in its ground state is given by

$$P_{\mathrm{Rb}} = \frac{n_\uparrow - n_\downarrow}{n_\uparrow + n_\downarrow}, \tag{1}$$

where $n_\uparrow$ ($n_\downarrow$) is the number of atoms with $m_J = +1/2\,(-1/2)$ in the Rb $5s\,^2S_{1/2}$ fine-structure level. This is equivalent to the Rb valence-electron polarization and is typically determined by Faraday rotation measurements [13,15]. In such a measurement, a linearly polarized probe beam well detuned from line center is passed through a cell of polarized vapor in a direction nearly parallel to the pumping beam. The angle of rotation of the linear polarization, $\Delta\varphi_p$, is measured to determine the polarization of the sample with the equation

$$P_{\mathrm{Rb}} = \frac{56\pi\delta(\Delta\varphi_p)}{3\lambda_0^2\Gamma_{\mathrm{nat}}LN}, \tag{2}$$

where N is the Rb number density, λ_0 is the Rb D_1 line-center wavelength, Γ_{nat} is the natural linewidth of the transition, L is the length over which the probe interacts with the vapor, and δ is the detuning of the probe-beam wavelength from the line center.

In such a measurement, the spin polarization is sampled along the entire length of the vapor through which the probe propagates. Thus Eq. (2) yields an average polarization along the cell length. Additionally, the measurement requires optical access through both ends of the vapor cell and can result in inconvenient configurations of optical elements in order to provide the necessary near-collinearity of the probe and pump beams.

We report here a simple heuristic method to determine the polarization of an optically pumped alkali-metal vapor, using a probe beam tuned to the D_1 transition and oriented perpendicular to the pump beam. This scheme is optically simple and has the advantage that it can provide spatially resolved polarization information in cells containing moderate Rb density.

II. METHOD

The experimental setup we used in this work is shown both schematically (Fig. 1) and in more detail (Fig. 2). A circularly polarized pump beam passed along the axis of a cylindrical vapor cell and was oriented parallel to an imposed magnetic field along the z quantization axis. A linearly polarized probe beam was directed through the side of the vapor cell, perpendicular to the pump beam. With a photodiode detector and digital oscilloscope, transmission vs frequency profiles were obtained for the probe beam with its polarization axis parallel to the z axis (π linear polarization) and with its polarization axis normal to both the pump and probe propagation directions (π_y linear polarization). Typical data for the probe transmission profile are shown in Fig. 3.

*Present address: Sloane Physics Laboratory, Yale University, New Haven, CT 06520.

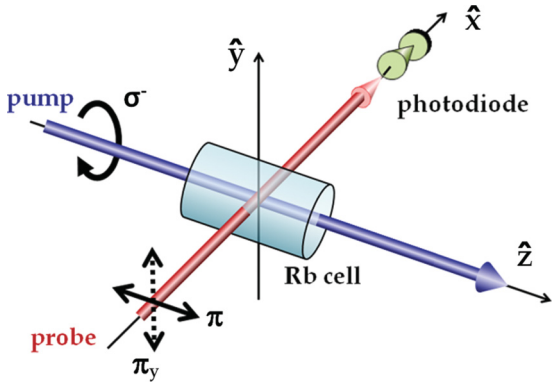

FIG. 1. (Color online) Schematic of the experimental setup. A circularly polarized beam propagating along the z axis optically pumps the alkali-metal vapor. A magnetic field is imposed along the z axis. The transmission of a linearly polarized, perpendicularly oriented probe beam is measured with a photodiode detector for two polarizations: π (polarization axis parallel to the z axis) and π_y (polarization axis parallel to the y axis).

The profile of the π probe was subtracted from that of the π_y probe to give a difference trace D which provides information about P_{Rb}. As seen in Fig. 3, two particularly prominent features in the difference profile correspond to π_y light being more strongly absorbed than π light near the ^{87}Rb $F = 2 \rightarrow F = 1$ transition and π light being more strongly absorbed than π_y light near the ^{85}Rb $F = 3 \rightarrow F = 3$ transition. The extrema of these features are referred to as D_{min} and D_{max}, respectively.

Figure 4 depicts the allowed atomic transitions for polarized light in the dipole approximation. If σ^+ (σ^-) circularly polarized light is absorbed by an atom, it will cause an electronic transition with $\Delta m_F = +1\,(-1)$. Linearly polarized π light drives a $\Delta m_F = 0$ transition, while π_y light drives a transition to a state which is a coherent superposition of $\Delta m_F = +1$ and $\Delta m_F = -1$ states.

The data of Fig. 3 can be explained qualitatively in the following way. Consider a Rb vapor for which we label the ground and excited states F_g and F_e, respectively. If the vapor

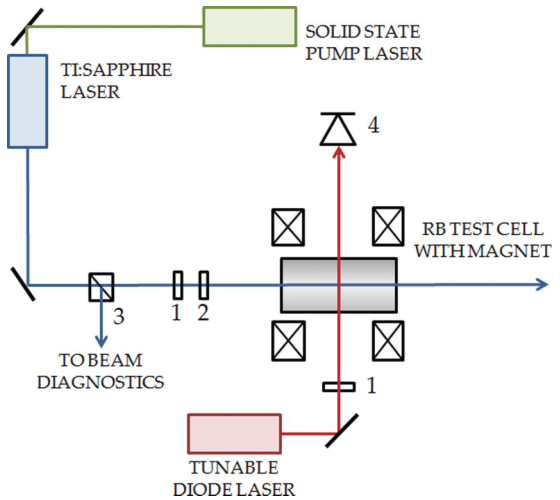

FIG. 2. (Color online) Apparatus details: (1) linear polarizer, (2) quarter-wave plate, (3) beam sampler, and (4) photodiode.

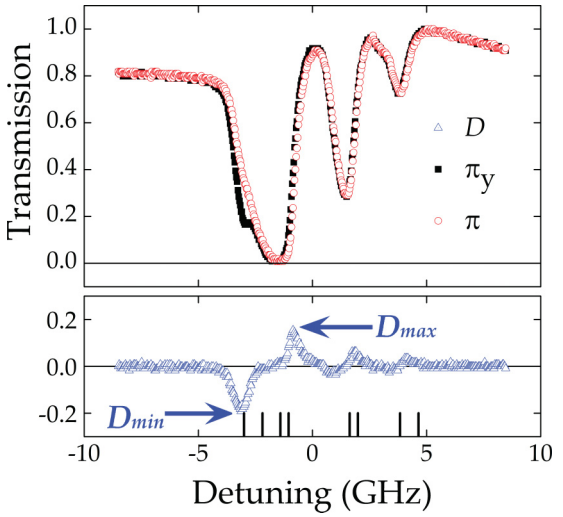

FIG. 3. (Color online) Measured transmission for transverse π_y and π light and the difference signal (D) for a Rb density of 2.4×10^{12} cm^{-3} with 10 Torr of N_2 buffer gas. The detunings from line center of the ground-to-excited hyperfine-level transitions are indicated at the bottom of the graph; from left to right: ^{87}Rb $F = 2 \rightarrow F = 1$, ^{87}Rb $2 \rightarrow 2$, ^{85}Rb $3 \rightarrow 2$, ^{85}Rb $3 \rightarrow 3$, ^{85}Rb $2 \rightarrow 2$, ^{85}Rb $2 \rightarrow 3$, ^{87}Rb $1 \rightarrow 1$, ^{87}Rb $1 \rightarrow 2$. The values of D_{min} and D_{max} are indicated.

is maximally polarized, with all atoms having $|m_F| = F$ in the ground state, the population will not affect a π-polarized probe beam tuned to a transition with $F_g > F_e$, but can absorb π_y light of the same frequency [Fig. 5(a)]. This explains the negative feature associated with D_{min} near the ^{87}Rb $F = 2 \rightarrow F = 1$ transition. Figure 5(b) illustrates the case of the probe tuned to a transition for which $F_g = F_e$ in the same spin-polarized vapor. For atoms having $m_F = +F$ ($m_F = -F$), absorption of the π_y light component giving the transition $\Delta m_F = +1$ ($\Delta m_F = -1$) is not allowed, but the absorption of π light displays no such suppression. Thus, the positive feature associated with D_{max} occurs near the ^{85}Rb $F = 3 \rightarrow F = 3$ transition.

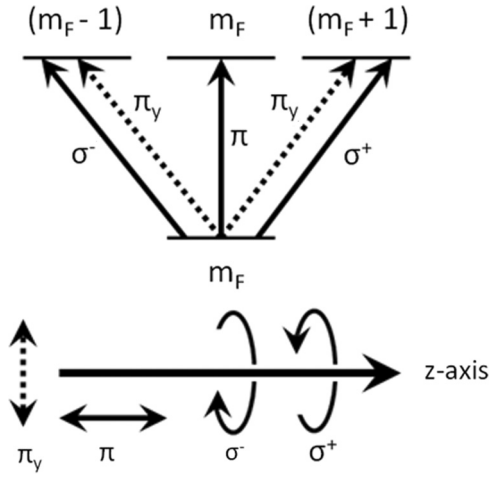

FIG. 4. Allowed atomic transitions for polarized light in the dipole approximation. The m_F states are those in the z-axis basis.

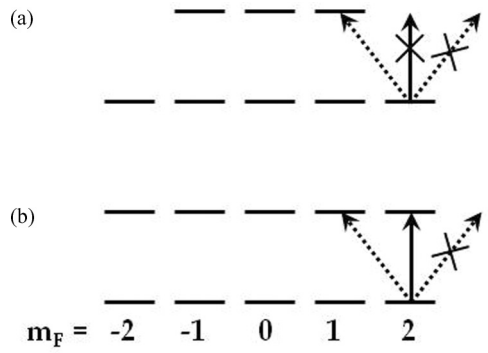

FIG. 5. Allowed and forbidden transitions (the latter crossed out) from the ^{87}Rb $F = 2$, $m_F = 2$ ground state to (a) the $F = 1$ excited state and (b) $F = 2$ excited state driven by linearly polarized transverse probe light. Transition designations as in Fig. 4.

III. ATOMIC ORIENTATION AND ALIGNMENT

In the excitation of atoms by light, two important quantities are the atom's orientation (O):

$$O = \frac{\sum_{m_F} m_F n_{m_F}}{\sqrt{F(F+1)}\sum_{m_F} n_{m_F}}, \tag{3}$$

a measure of its magnetic dipole moment, and alignment (A):

$$A = \frac{\sum_{m_F} \left[3m_F^2 - F(F+1)\right] n_{m_F}}{F(F+1)\sum_{m_F} n_{m_F}}, \tag{4}$$

a measure of its electric quadrupole moment [16,17]. In the above equations, m_F and F are the usual quantum state numbers for the atom's total angular momentum, and n_{m_F} is the population of the state with m_F. Equation (3) is equivalent to Eq. (1), but with hyperfine states now shown explicitly. For an oriented atom, the state populations with $+m_F$ differ from those with $-m_F$. On the other hand, an aligned atom has unequal populations for different $|m_F|$ values [18]. Optical pumping of an alkali-metal vapor with circularly polarized light will generally result in both an alignment and orientation of the atoms. However, a vapor pumped with σ^+-polarized light will have the same alignment as a vapor pumped with σ^--polarized light. Therefore, the $|m_F|$ distribution, i.e., alignment, is independent of pump helicity.

For both π and π_y light, the probability of photon absorption is independent of the sign of m_F [19]. Thus, monitoring their relative absorption yields information about the alignment of the sample, not its orientation. Indeed, our method cannot determine the sign of P_{Rb}. It is akin to measurement of the linear polarization (Stokes parameters P, P_1, M/I, Q/I, S_1/S_0, η_3, etc.) of fluorescence produced in a cylindrically symmetric collision geometry, which uniquely determines alignment [16]. It is different because it is affected by absorption of the probe laser.

There are multiple population distributions yielding a given sample orientation, and likewise there are multiple ways to get a particular alignment. Thus, a one-to-one mapping between orientation and alignment does not exist. Consider, for example, a possible time evolution of state populations tending towards 100% polarization, illustrated in Fig. 6. In this scheme, the population migrates to a final extreme value

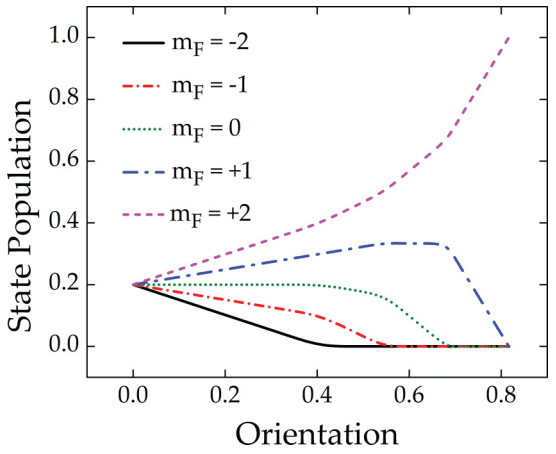

FIG. 6. (Color online) A possible evolution of state populations from an initially unpolarized state to a final, maximally polarized one.

of m_F in such a way that, for the populated states, $n_{m_F+1} - n_{m_F}$ is constant. Figure 7 shows the alignment of this example as a function of its orientation. On the same graph is shown the alignment vs orientation for a sample where the dominant process is spin exchange, a system that can be described by a spin temperature [20] common in some regimes of optical pumping. The graph also displays the near-linear relationship between orientation and alignment that occurs with optical pumping under our conditions, derived from the individual Zeeman sublevel populations found with numerical calculations (described below). We note that, although it is fortunate that we are working in a regime where the orientation and alignment are almost proportional, this condition is not necessary for side probing to serve as a useful indicator of orientation (and therefore P_{Rb}); the relationship between orientation and alignment will simply take a different functional form.

IV. EXPERIMENTAL DETAILS

A ∼10 W beam from a Coherent Verdi laser was used to pump a Spectra Physics 3900 Ti:sapphire laser (Fig. 2). The output of the 3900 laser, used to pump the Rb vapor, was

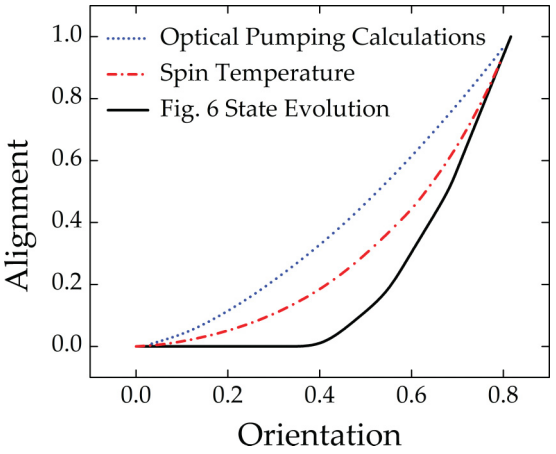

FIG. 7. (Color online) Correlation between alignment and orientation for three different state-population evolution schemes.

$\sim$1 mm in diameter with a typical power of 800 mW. Its spectral profile was "trident shaped" comprising three laser cavity modes equally spaced $\sim$200 MHz apart. This beam passed through a clean-up linear polarizer and quarter-wave plate before entering the cylindrical test cell containing Rb vapor of natural isotopic abundance. The cell was 4.3 cm long and 2.5 cm in diameter and contained 10 Torr of N_2 buffer gas. A magnetic field of strength $\sim$1 mT was applied by electromagnets along the direction of the pump beam to maintain the orientation of the polarized Rb. The pump beam was carefully aligned to within 2° of the magnetic field direction, detuned positively ($\sim$2 GHz) from the center of the D_1 transition, and circularly polarized to >99.5% to avoid the polarization-reversal effect that has been observed in some systems lacking a "repump" laser [11,21]. The temperature of the Rb cell was varied to alter N, and P_{Rb} was changed by adjusting the power of the pump laser beam. Both P_{Rb} and N were measured with Faraday rotation techniques [13,15] and therefore represent quantities averaged over the cell length along the z axis. We estimate the systematic uncertainty in both measurements to be $\sim$10% due to the fact that we occasionally made measurements of polarization as high as 110%. Because polarization is inversely proportional to density, we assign the same uncertainty to our density measurements.

The probe laser (New Focus tunable diode Vortex laser, model 6017) had a spectral width of $\sim$300 kHz. Its power was typically reduced to $\sim$20 μW. Using an infrared-sensitive camera, optimal overlap of pump and probe beams was achieved by comparing images of the cell when the pump was blocked and unblocked. Additionally, a separate investigation of P_{Rb} as a function of radial distance from the pump beam revealed that the probe was well within the region of maximum polarization.

Transmission profiles were obtained for both the π and π_y beam polarizations (Fig. 3). When scanning the probe frequency, the power varied somewhat, and the transmission changed due to etalon effects of the glass cell walls. This did not affect the overall results. The transmission signal was normalized to the maximum value of the unabsorbed beam intensity occurring just to the right of the ^{87}Rb $F = 1 \rightarrow F = 2$ transition.

V. MODEL CALCULATIONS

To understand more quantitatively the relative absorption of the π- and π_y-polarized probe across the frequency span, it is necessary to incorporate the sublevel-to-sublevel relative transition probabilities of the different polarizations [22]. The system was thus modeled by solving rate equations to describe each F, m_F ground- and excited-state sublevel for ^{85}Rb and ^{87}Rb, and the transmission of the transverse probe beam for each polarization state was calculated. These rate equations included the optical pumping process by the pump beam, spontaneous emission, spin relaxation, and optical pumping by the probe beam. We used the interpretive language MATHEMATICA to solve the rate equations. A sample equation for ^{87}Rb for one ground-state sublevel population n_1, where $n_1 = n(^2S_{1/2}, F = 2, m_F = -2)$, and a probe polarization of π_y is

$$\frac{\partial n_1}{\partial t} = \Gamma_{\mathrm{pump2}\rightarrow 2}\frac{(2n_b - 2n_1)}{4} + \Gamma_{\mathrm{pump2}\rightarrow 1}\frac{(6n_h - 6n_1)}{4} + A_{\mathrm{Einstein}}\frac{(4n_a + 2n_b + 6n_h)}{12} + \Gamma_{\mathrm{mix}}\left(\frac{N}{8} - n_1\right) + \Gamma_{\mathrm{probe2}\rightarrow 2}\frac{(2n_b - 2n_1)}{8} + \Gamma_{\mathrm{probe2}\rightarrow 1}\frac{(6n_h - 6n_1)}{8}. \quad (5)$$

Here, $n_b = n(^2P_{1/2}, F = 2, m_F = -1)$, $n_h = n(^2P_{1/2}, F = 1, m_F = -1)$, and $n_a = n(^2P_{1/2}, F = 2, m_F = -2)$, A_{Einstein} is the spontaneous decay rate of Rb, and a spin relaxation rate is Γ_{mix}. The optical pumping rate $\Gamma_{\mathrm{pump2}\rightarrow 2}$ was calculated with an integral combining the spectral profile of the laser and a Voigt profile convolution of the Doppler-broadened Gaussian line shape and collisionally broadened Lorentzian line shape. Its value took into account the center frequency of the laser and the excited-state $F = 2$ level to ground-state $F = 2$ level frequencies. The other optical pump rates $\Gamma_{\mathrm{pump2}\rightarrow 1}$, $\Gamma_{\mathrm{probe2}\rightarrow 2}$, and $\Gamma_{\mathrm{probe2}\rightarrow 1}$ were defined similarly. Thus, we used 16 equations to describe each of the ground- and excited-state sublevels of ^{87}Rb and 24 equations to describe ^{85}Rb, along with the normalization forcing the sum of all populations to equal N.

The calculations were simplified with a number of assumptions. Spin-exchange collisions [21,23,24] within and between the isotopes were neglected; modeling the pumping with a broadband laser on atoms collisionally broadened by the buffer gas sufficiently describes the polarization of both isotopes [25,26]. Previous work with this system indicates that 10 Torr of N_2 buffer gas substantially reduces problems associated with radiation trapping [12,13], so such effects were not considered. The pump and probe lasers were approximated with spectrally flat beams of width 550 MHz and 300 kHz, respectively, and their intensities were taken to be spatially flat in both radius and depth into the cell. We neglected individual velocity subgroups and described each atom with the Voigt profile idealized absorption line shape. The spin relaxation rate is the beam-crossing rate for atoms in vacuum joined smoothly to the beam-crossing rate for atoms diffusing in the presence of N_2 gas to account for the transition from the molecular flow to diffusion regimes. Since spin-exchange collisions are not very important and we assumed a spatially flat laser profile, our calculated populations are independent of N.

An example of the calculations of the transmission of the two orthogonal probe polarizations and the resultant D curve is shown in Fig. 8. The calculations nicely reproduce the main features of the difference curve, including the negative- and positive-going peaks associated with D_{min} and D_{max}.

VI. RESULTS

The goal of this work was to find a simple, useful way to map out and monitor the polarization of an alkali-metal vapor. While our calculations reproduce the major features of the D curve in Fig. 3, it would be inconvenient to do real-time modeling of entire scans of both probe polarizations in order to extract values of P_{Rb}. Thus, we present a more heuristic method to determine the polarization using D_{min} and/or D_{max} and their

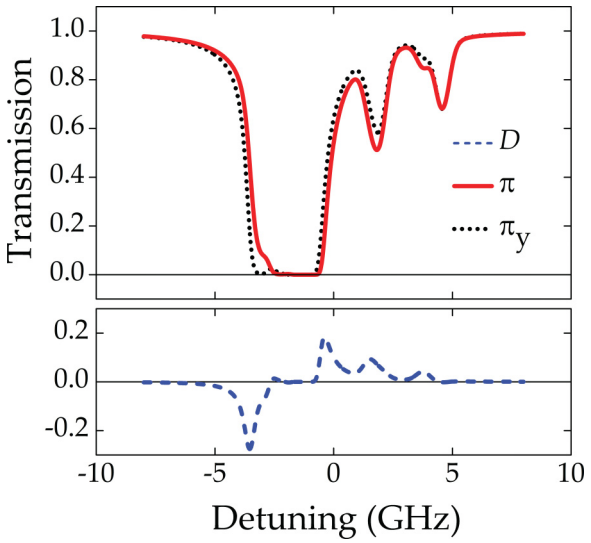

FIG. 8. (Color online) Calculated transmission curves for a transverse 20 μW probe with polarizations π_y and π along with their difference curve D. The calculations are for $N = 1.4 \times 10^{12}$ cm^{-3} and $P_{\mathrm{Rb}} = 73\%$ in a cell of diameter 2.5 cm with 10 Torr N_2 buffer gas.

correlation with P_{Rb}. We choose not to use the features that occur at positive detunings since they are inherently smaller and can exhibit complex behavior caused by the pump laser being in the same frequency range. In fact, in the limit of perfect Rb polarization, these features disappear altogether because they represent transitions out of the lower F level of the ground state, which is actively depleted by the optical pumping process.

The quantity D_{min} is plotted vs P_{Rb} and is displayed in Fig. 9 along with values of D_{min} obtained from our model. Seven values of N between 10^{12} and 10^{13} cm^{-3} were investigated. For clarity, the results from only four densities are plotted; the remaining data are consistent with those shown. Our model fitted the data better if we used N values twice what

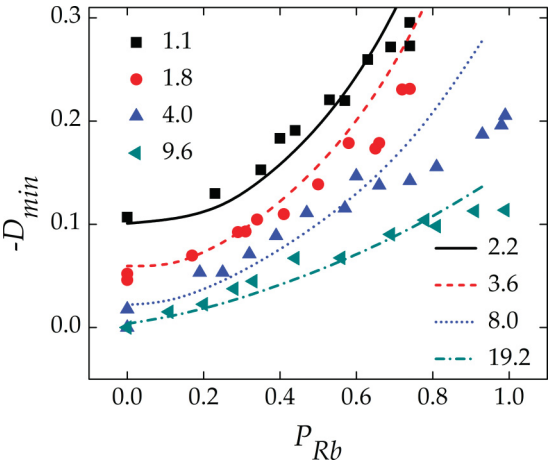

FIG. 9. (Color online) The negative of D_{min} plotted vs P_{Rb} as measured by longitudinal Faraday rotation. The curves show our calculations of D_{min}; the symbols correspond to our measurements with densities half those used in the calculations. Densities indicated in the legend are in units of 10^{12} cm^{-3}.

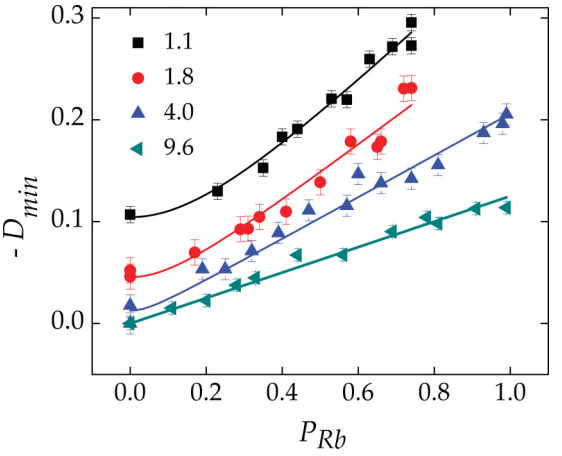

FIG. 10. (Color online) The negative of D_{min} plotted vs P_{Rb} measured by longitudinal Faraday rotation. A best-fit curve for each density using Eq. (6) yielded the fit coefficients $D_{\mathrm{min}}(P_{\mathrm{Rb}} = 0)$ and A plotted in Fig. 11. Densities indicated in the legend are in units of 10^{12} cm^{-3}.

we measured, indicating N variation in the cell or a current problem with the model.

The two quantities P_{Rb} and D_{min} exhibit an approximately linear relationship, although for lower N the simple linear dependence fails at lower polarizations, yielding a nonzero value of the intercept, $D_{\mathrm{min}}(P_{\mathrm{Rb}} = 0; N)$. Notwithstanding this complication, a method to determine P_{Rb} by heuristically fitting the D_{min} data for a given N is suggested by the results of Fig. 9. Hyperbolic fits of the form

$$D^2_{\mathrm{min}}(P_{\mathrm{Rb}}, N) = D^2_{\mathrm{min}}(P_{\mathrm{Rb}} = 0; N) + P^2_{\mathrm{Rb}} A^2(N) \qquad (6)$$

adequately estimate D_{min} for our particular set of experimental parameters (Fig. 10). [Note that Eq. (6) can easily be rearranged to obtain P_{Rb} as a function of D_{min}.] To estimate the statistical uncertainties of our measurements, we assign a common uncertainty to the difference-signal data for a given density to provide a reduced χ^2 value equal to 1 for the fit. This value is then used to calculate the uncertainties of the hyperbolic-fit coefficients $D_{\mathrm{min}}(P_{\mathrm{Rb}} = 0; N)$ and $A(N)$ shown in Fig. 11.

The utility of this technique is limited by the size of the cell and the intensity of the probe beam. For $N\sigma_\lambda d \gg 1$, where σ_λ is the absorption cross section at wavelength λ and d is the cell diameter, both polarizations are almost completely absorbed and their transmission difference becomes small compared to the experimental noise. Conversely, for $N\sigma_\lambda d \ll 1$, there is not enough absorption to reliably measure a difference signal. Experiments could easily be designed to obviate these problems.

Figure 11 shows the intercept $D_{\mathrm{min}}(P_{\mathrm{Rb}} = 0; N)$ and the asymptotic slope $A(N)$ of the hyperbolic fits for the data set shown in Fig. 10. For our experimental conditions, the N dependence of these coefficients can be described empirically by

$$D_{\mathrm{min}}(P_{\mathrm{Rb}} = 0; N) = \frac{1}{E + FN} \qquad (7)$$

and

$$A(N) = \frac{1}{G + HN}, \qquad (8)$$

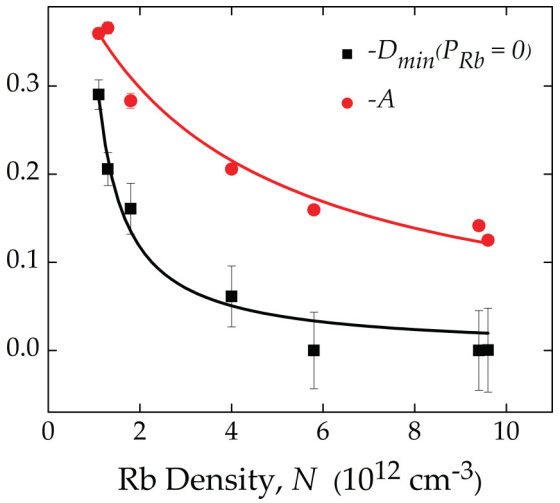

FIG. 11. (Color online) Dependence of fit coefficients $-D_{\min}(P_{\mathrm{Rb}} = 0)$ and $-A$ from Eq. (6) vs Rb density. The fits shown above correspond to Eqs. (7) and (8).

where $E = 2.7 \pm 1.7$, $F = -5.6 \pm 1.5$ cm^3, $G = -2.07 \pm 0.05$, and $H = -0.64 \pm 0.02$ cm^3, and N is measured in units of 10^{12} cm^{-3}. Equations (7) and (8) allow determination of the polarization based upon measured values of $D_{\min}$ and N. Different experimental configurations would of course require different fitting parameters.

Both $D_{\min}(P_{\mathrm{Rb}} = 0; N)$ and $D_{\min}(P_{\mathrm{Rb}} = 1.0; N)$ are decreasing functions of number density in our experiment. At low densities, these quantities would be expected to increase with increasing N, and our model calculations confirm this. However, since our measurements are based upon a transmission signal near the D_1 absorption lines, all the probe light is absorbed for high N. Thus, the signal is attenuated and the values of $D_{\min}(P_{\mathrm{Rb}} = 0)$ and $D_{\min}(P_{\mathrm{Rb}} = 1.0)$ are reduced to zero, as shown in Fig. 12.

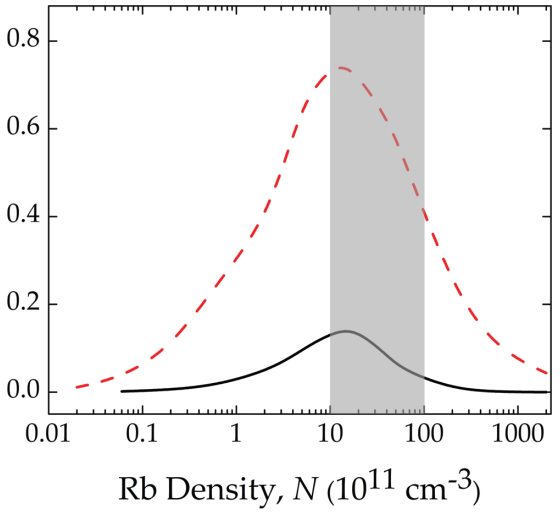

FIG. 12. (Color online) The values of $-D_{\min}(P_{\mathrm{Rb}} = 0)$ (solid line) and $-D_{\min}(P_{\mathrm{Rb}} = 1.0)$ (dashed line) as a function of N for 50 μW probe power. The shaded area corresponds to the range of densities used in our experiments.

It is desirable to understand and eliminate the nonzero values of $D_{\min}(P_{\mathrm{Rb}} = 0)$. This behavior initially surprised us. The value of $D_{\min}$ is directly related to the atomic alignment in the system, as discussed earlier, but what causes this alignment in the absence of a pump beam? Although it is true that the longitudinal magnetic field breaks the y, z symmetry of the experiment, it is too weak ($\sim$1 mT) to produce the alignment we observe by itself. In other words, $kT \gg \Delta E$, where ΔE is a characteristic Rb Zeeman energy shift. We note that, strictly speaking, in the absence of any laser-driven process, a magnetic field, which is a pseudovector, must cause orientation.

In fact, $D_{\min}(P_{\mathrm{Rb}} = 0) \neq 0$ in the absence of a pump beam is caused by the probe itself. (This is different from the orientation caused by an intense, linearly polarized side pump beam in the Paschen-Back regime [27].) When the probe is tuned to the ^{87}Rb $F = 2 \rightarrow F = 1$ transition [Fig. 5(a)] with π polarization, it can pump the atoms into the stretched state, or "hollow out" the z-basis m_F ground-state distribution for ^{87}Rb $F = 2$ atoms, leaving only m_F values equal to $\pm F$. At this transition frequency, the sample would become transparent to the π probe, but the π_y probe can always be absorbed. This differential absorption yields the nonzero $D_{\min}(P_{\mathrm{Rb}} = 0)$. Ground-state populations are maintained by the longitudinal (z-axis) magnetic field, which holds atoms in a given z basis m_F state once they reach it by a photonic transition. This is equivalent to the classical picture of magnetic m_F dipoles precessing about the magnetic field. Only in the cases of a magnetic field aligned along $\hat{y} \pm \hat{z}$ or one that vanishes (i.e., is so small that any precession time is much longer than a characteristic depolarization time) will $D_{\min}(P_{\mathrm{Rb}} = 0)$ approach zero in the absence of a pump beam.

These considerations lead to two ways to avoid the offset of $D_{\min}(P_{\mathrm{Rb}} = 0)$ for measurements of low polarizations. First, a probe of very low intensity would not interfere with the polarization measurement. Figure 13 shows the result of our model calculation indicating that $D_{\min}(P_{\mathrm{Rb}} = 0)$ approaches zero at sufficiently low probe powers. The detection sensitivity and the quality and curvature of our cell walls required probe intensities in the regime where the $D_{\min}$ intercept became measurable, but experiments could be

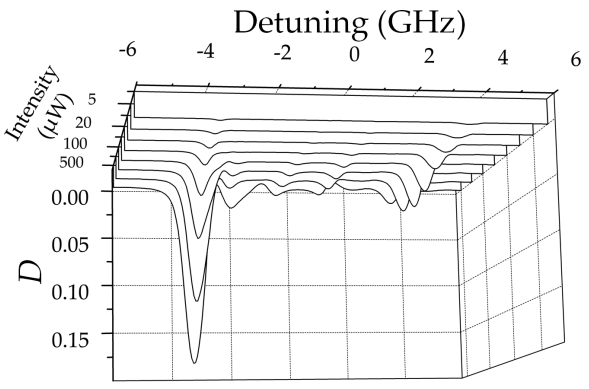

FIG. 13. A sample of graphs showing the calculated value of the difference function D as a function of the probe laser detuning for a span of probe laser powers in the absence of a pump beam for $N = 4 \times 10^{12}$ cm^{-3}. The minimum value of each curve corresponds to $D_{\min}$.

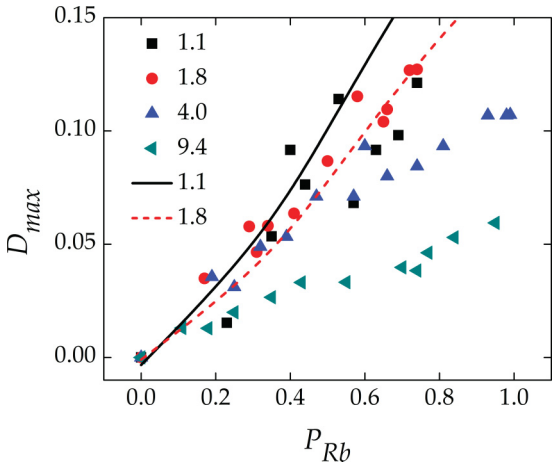

FIG. 14. (Color online) The maximum value of the difference signal, $D_{\max}$, plotted vs P_{Rb} measured by longitudinal Faraday rotation. The curves show calculations of $D_{\max}$. Densities indicated in the legend are in units of 10^{12} cm^{-3}.

designed with much lower probe intensities than those shown here.

A second way to eliminate the offset would be to choose a feature on the difference curve where the probe beam does not optically pump the sample, such as at $D_{\max}$. The ^{85}Rb $F = 3 \rightarrow F = 3$ transition does not allow the probe to create a dark state for either π or π_y polarization. Figure 14 shows experimental data and model calculations for the use of $D_{\max}$ to predict polarization. The results display a signal directly proportional to P_{Rb} without any offset at low P_{Rb}, even at probe laser intensities problematic for $D_{\min}$ measurements. Unfortunately, the model for $D_{\max}$ fails at higher densities where the location of $D_{\max}$ becomes ambiguous among the multiple positive peaks in the D curve. In future work we plan to study the efficacy of a $D_{\max}$ method more thoroughly.

Either a low probe power or use of $D_{\max}$ ensures a zero-intercept value of D for $P_{\mathrm{Rb}} = 0$, enabling a measurement of P_{Rb} with a single N-dependent slope parameter. Having a signal directly proportional to P_{Rb} also opens the possibility of measurements fast enough to perform real-time tuning of P_{Rb} or mapping of the transverse spatial variation of P_{Rb}.

VII. CONCLUSION

We have demonstrated a heuristic method to determine P_{Rb} of an optically pumped vapor by analyzing the difference of transmission for orthogonally linearly polarized probe beams oriented perpendicular to the quantization axis. This transmission difference is understood qualitatively by considering the allowed photonic transitions for an atomic vapor that is polarized and quantitatively by detailed modeling of the polarized vapor with relevant rate equations. For measuring P_{Rb}, a system of given dimensions, buffer-gas pressure, N, and probe intensity would first need calibration or modeling in order to determine P_{Rb} as a function of $D_{\min}$ or $D_{\max}$. This scheme has advantages over traditional Faraday rotation in that it is relatively simple to set up and is compact. The method could map the spatial variation of the polarization in a cell, enables a polarization measurement if the cell is not accessible at both ends along the z axis, and offers the potential of a fast, real-time indicator for optimizing the polarization of a sample.

ACKNOWLEDGMENTS

The authors acknowledge helpful discussions with Herman Batelaan. This work was supported by NSF Grant No. PHY-0855629 approved under Los Alamos Release LA-UR-12-24475.

[1] D. F. Phillips, A. Fleischhauer, A. Mair, R. L. Walsworth, and M. D. Lukin, Phys. Rev. Lett. **86**, 783 (2001).
[2] A. D. Ludlow *et al.*, Science **319**, 1805 (2008).
[3] S. J. Smullin, I. M. Savukov, G. Vasilakis, R. K. Ghosh, and M. V. Romalis, Phys. Rev. A **80**, 033420 (2009).
[4] L. W. Anderson, Nucl. Instrum. Methods **167**, 363 (1979).
[5] C.-J. Liu, N. B. Mansour, Y. Azuma, H. G. Berry, D. A. Church, and R. W. Dunford, Phys. Rev. Lett. **64**, 1354 (1990).
[6] A. Zelenski, Rev. Sci. Instrum. **81**, 02B308 (2010).
[7] G. L. Jones *et al.*, Physica B **356**, 86 (2005).
[8] K. Ishikawa, B. Patton, Y.-Y. Jau, and W. Happer, Phys. Rev. Lett. **98**, 183004 (2007).
[9] J. Alcorn *et al.*, Nucl. Instrum. Methods Phys. Res., Sect. A **522**, 294 (2004).
[10] T. G. Walker and W. Happer, Rev. Mod. Phys. **69**, 629 (1997).
[11] E. B. Norrgard, D. Tupa, J. M. Dreiling, and T. J. Gay, Phys. Rev. A **82**, 033408 (2010).
[12] H. Batelaan, A. S. Green, B. A. Hitt, and T. J. Gay, Phys. Rev. Lett. **82**, 4216 (1999).
[13] M. A. Rosenberry, J. P. Reyes, D. Tupa, and T. J. Gay, Phys. Rev. A **75**, 023401 (2007).
[14] F. Gong, Y.-Y. Jau, and W. Happer, Phys. Rev. Lett. **100**, 233002 (2008).
[15] Z. Wu, M. Kitano, W. Happer, M. Hou, and J. Daniels, Appl. Opt. **25**, 4483 (1986).
[16] U. Fano and J. H. Macek, Rev. Mod. Phys. **45**, 553 (1973).
[17] M. Auzinsh, D. Budker, and S. M. Rochester, *Optically Polarized Atoms: Understanding Light-Atom Interactions* (Oxford University Press, New York, 2010).
[18] C. H. Greene and R. N. Zare, Annu. Rev. Phys. Chem. **33**, 119 (1982).
[19] M. Kraińska-Miszczak, J. Phys. B **12**, 555 (1979).
[20] L. W. Anderson, F. M. Pipkin, and J. C. Baird, Phys. Rev. **120**, 1279 (1960).
[21] M. V. Romalis, Phys. Rev. Lett. **105**, 243001 (2010).
[22] H. J. Metcalf and P. van der Straten, *Laser Cooling and Trapping* (Springer, New York, 1999).
[23] D. R. Swenson, D. Tupa, and L. W. Anderson, J. Phys. B **18**, 4433 (1985).
[24] B. Lancor and T. G. Walker, Phys. Rev. A **83**, 065401 (2011).
[25] D. Tupa, L. W. Anderson, D. L. Huber, and J. E. Lawler, Phys. Rev. A **33**, 1045 (1986).
[26] D. Tupa and L. W. Anderson, Phys. Rev. A **36**, 2142 (1987).
[27] C. Martin, T. Walker, L. W. Anderson, and D. R. Swenson, Nucl. Instrum. Methods Phys. Res., Sect. A **335**, 233 (1993).